Rocznik Ochrona Środowiska

Volume 28 Year 2026 ISSN 2720-7501 pp. 673-687

https://doi.org/10.54740/ros.2026.045 open access

Received: July 2026 Accepted: September 2026 Published: September 2026

Sustainable Goat Bone-Derived Hydrochar as an Efficient Adsorbent for Malachite Green Removal: Adsorption Performance, Mechanism, and Surface Characterization

Bharati Patil[1], Mohammad Yusuf[2], Tripti Gupta[3*], Zaid Abdulhamid Alhulaybi Albin Zaid[2], Abdulrazak Jinadu Otaru[2], Sagar Kolekar[4*]*

[1]*Department of Applied Science, Yeshwantrao Chavan College of Engineering, Nagpur, India*

[2]*Department of Chemical Engineering, College of Engineering, King Faisal University, Al Ahsa, Saudi Arabia*

[3]*Department of Civil Engineering, Ramdeobaba University*

(Shri Ramdeobaba College of Engineering & Management) Nagpur, India

[4]*Symbiosis Institute of Technology (SIT), Symbiosis International (Deemed University), Pune, India*

**corresponding author's e-mail: sagar.kolekar@sitpune.edu.in, myusuf@kfu.edu.sa, guptatb@rbunagpur.in*

Abstract: Due to the accumulation of synthetic dyes in water bodies, it is important to develop efficient and sustainable adsorbents from renewable waste resources. The hydrothermal carbonization of waste goat bones (WGB) was successfully carried out to produce goat bone hydrochar powder (GBHP), which was used to remove malachite green (MG) from aqueous solution. BET, FESEM, XRD, FTIR, and Raman spectroscopy were used to investigate the structural and surface properties of GBHP. The prepared hydrochar had a high specific surface area of 16.8 m^2/g, an average pore diameter of 4.6 nm, and a pore volume of 0.139 cm^3/g, which are ideal for creating many available hydrochar adsorption sites. The optimum conditions for batch adsorption experiments were found to be 40 mg L^{-1} initial MG concentration, 1.5 g adsorbent dosage, pH 6, 90 min contact time, and 308 K, with nearly 97% removal of dye. This adsorption behavior was well described by the pseudo-second-order kinetic model ($R^2 = 0.9901$) and the Langmuir isotherm, indicating monolayer adsorption onto energetically uniform active sites. The negative Gibbs free energy of adsorption ($\Delta G° = -2.690$ to -2.651 kJ mol^{-1}) and exothermic nature ($\Delta H = -3.451$ kJ mol^{-1}) of the process were obtained from thermodynamic evaluation. The adsorption of MG was shown to be controlled by a combination of pore filling, hydrogen bonding, electrostatic attraction, π–π interactions and surface complexation as revealed by spectroscopic and morphological analyses. The results of this study indicate that goat bone hydrochar is a promising waste-based adsorbent and offer a feasible strategy for converting slaughterhouse waste into value-added materials for sustainable wastewater treatment.

Keywords: goat bone hydrochar, hydrothermal carbonization, malachite green, adsorption

1. Introduction

Rapid industrial expansion, coupled with accelerating urban development, has markedly increased the generation of wastewater rich in pollutants worldwide. In this group, dyes are among the most persistent because of their complex aromatic molecular structure, high molecular stability, resistance to microbial degradation, and recalcitrant nature under natural environmental conditions. It is estimated that a variety of dyes are available worldwide (Li et al., 2024; Shukla et al., 2024). It is estimated that these dyes are lost during various industrial processes and eventually end up in wastewater streams across the textile, paper, leather, printing, plastic, cosmetic, pharmaceutical, and aquaculture industries (Muteeb, Ansari, et al., 2025; Muteeb, Alshoaibi, & Ansari, 2025). Even at low levels below 1 mg L^{-1}, dyes are readily visible in water bodies. They will have a large impact on light transmittance, which will affect photosynthesis, dissolved oxygen levels, disruption of aquatic food chains, and decrease ecosystem productivity (Awad et al., 2019; Bushraet al., 2021; Clark et al., 1983). Furthermore, the presence of dye molecules and their degradation by-products has been associated with acute and chronic toxicological impacts, including mutagenicity, teratogenicity, genotoxicity, endocrine disruption, and carcinogenicity, highlighting the need for effective wastewater treatment processes (Hussain et al., 2021).

Malachite Green (MG) is a basic synthetic dye that has received considerable attention due to its widespread industrial use and its excellent persistence in the environment (Morris et al., 2024). Malachite green is a cationic triphenylmethane dye that has been widely used in the dyeing of textiles, silk and wool dyeing, leather dyeing, food packaging, printing and paper dyeing due to its high water solubility, brilliant colour, excellent tinctorial strength and relatively low production cost (Arunprasath et al., 2019; Bian et al., 2025). In addition to industrial uses, MG has been traditionally used in aquaculture as an antifungal, antiparasitic, and antimicrobial agent to control fungal infections and protozoan diseases in fish. The release of untreated effluents containing MG into the aquatic environment, however, has raised serious concerns regarding both the environment and public health. Malachite green has a very long environmental persistence due to its highly conjugated aromatic structure and exceptional chemical stability, leading to poor biodegradability (Arunprasath et al., 2019; Morris et al., 2024).

Furthermore, MG can be bio-transformed to the reduced derivative, leucomalachite green (LMG), which possesses enhanced environmental persistence and a higher bioaccumulation potential (Razia et al., 2025). Several toxicological studies have shown cytotoxic, genotoxic, mutagenic, teratogenic, hepatotoxic, nephrotoxic, and carcinogenic effects of prolonged exposure to MG and its metabolites in aquatic organisms and mammals. As a result, it is now banned or highly restricted in many countries for use in aquaculture production systems for food, highlighting the need for highly effective technologies to remove malachite green from contaminated wastewater before discharge into the environment (Bian et al., 2025).

Various physicochemical, biological, and advanced oxidation processes have been investigated for the removal of synthetic dyes. These techniques are coagulation–flocculation, chemical precipitation, membrane filtration, electrochemical oxidation, ozonation, photocatalysis, biodegradation, advanced oxidation processes (AOPs), and Fenton-based oxidation systems. Although many of these methods can show good dye removal efficiencies under laboratory conditions, several factors make their application at a large scale not feasible, including high operational and maintenance costs, high energy consumption, fouling of the membranes, complex reactor configurations, sludge formation, catalyst deactivation, incomplete mineralisation of pollutants and toxic secondary products formed. Therefore, the development of treatment systems with high removal efficiency, simplicity, environmental friendliness, economic viability, and long-term sustainability is a constant need (He et al., 2023; Kumar et al., 2025). Adsorption has emerged as the most efficient and widely adopted method owing to its operational simplicity, fast treatment kinetics, high removal efficiency over a wide concentration range, minimal or no production of secondary pollutants, easy regeneration, and its ability to be used in both batch and continuous treatment systems. The adsorption process involves many physicochemical interactions between the adsorbate molecules and the surface of the adsorbent, such as electrostatic attraction, hydrogen bonding, π–π electron donor–acceptor interactions, van der Waals interactions, pore-filling, hydrophobic interaction, ion exchange, acid–base interactions, and surface complexation. Thus, physicochemical properties such as surface area, functional groups, pore volume, size distribution, surface charge, crystallinity and chemical composition, contribute for efficient adsorption (Morris et al., 2024). Hence, many efforts have been made in the design of low cost, green and highly efficient adsorbents using naturally abundant biomass, agricultural waste, industrial waste and animal waste (Beulah & Muthukumaran, 2020; Bian et al., 2025; Ledakowicz & Paździor, 2021).

Waste valorization technologies using biomass conversion have become more popular in recent years and offer an effective strategy for simultaneously addressing both solid waste management and wastewater remediation (Inala & Choksi, 2025). Animal bone waste is a very promising raw material for adsorbent production because of its availability, negligible economic value, good mechanical stability, and unique inorganic composition. Animal bones contain calcium phosphate, hydroxyapatite, calcium carbonate, carbonaceous matter derived from collagen, and other trace minerals (Khan A.M. et al., 2023). All these constituents create many chemically active adsorption sites that can interact with organic contaminants via electrostatic attraction, ion exchange, ligand exchange, hydrogen bonding, coordination interactions, and surface complexation (Boakye et al., 2024). Furthermore, the hierarchical porous structure is a pre-existing characteristic of bone matrices and promotes efficient mass transfer and the diffusion of pollutant molecules to adsorption sites, thereby improving adsorption kinetics and capacity. Hydrothermal carbonization (HTC), a thermochemical conversion process, has emerged as an eco-friendly technology for improving the adsorption properties of bone-derived materials to produce hydrochar. While pyrolysis is usually performed at temperatures > 500°C in an oxygen-limited atmosphere, hydrothermal carbonization is carried out in subcritical water at relatively low temperatures (180–250°C) at autogenous pressure (Jankovská et al., 2025; Pasipanodya et al., 2024). Dehydration, decarboxylation, condensation, polymerization, and aromatization reactions occur concurrently during the HTC process, leading to the formation of oxygen-rich active site groups, improved carbonaceous structures, increased structural stability, and the development of a porous morphology. Moreover, hydrothermal carbonization reduces energy demand, as wet biomass can be used directly without prior drying, which is particularly relevant for the utilization of high-moisture biological wastes to produce functional adsorbent materials. The resulting hydrochar typically has enhanced surface chemistry, porosity, surface reactivity, and chemical stability (Durak et al., 2026; Inala & Choksi, 2025).

Goat bones are by-products from slaughterhouses, are readily available, and are produced in large quantities worldwide due to the ever-increasing meat consumption, along with other animal-derived wastes (Limeneh et al., 2022). Goat bones have a high mineral content and economic value. Still, they are often landfilled or disposed of in uncontrolled ways, which can lead to odour production, microbial growth, greenhouse gas emissions, and other environmental impacts. Thus, converting goat bone waste into hydrochar is a sustainable waste management system that not only alleviates environmental pollution but also produces value-added adsorbent materials (Hart et al., 2023; Limeneh et al., 2022). Furthermore, the synergistic adsorption behavior of a mixture of hydroxyapatite minerals and carbonaceous phases in goat bone hydrochar, driven by multiple adsorption

mechanisms, could increase the removal efficiency of cationic organic pollutants such as malachite green. While some studies have reported using various adsorbents such as activated carbons, agricultural biomass, biochars, metal oxides, clay minerals, polymer composites, and waste-derived adsorbents for adsorption of malachite green, very few studies have been conducted on hydrothermally synthesized goat bone hydrochar (Hart et al., 2022; Pasipanodya et al., 2024). Likewise, systematic studies that combine structural characterization with adsorption kinetics, adsorption equilibrium isotherms, adsorption thermodynamic studies, adsorption mechanisms, and regeneration studies are still limited; hence, more studies are warranted to shed light on the adsorption mechanism of malachite green onto goat bone hydrochar (Abioye, Falua et al., 2025).

The present study is designed to develop a sustainable GBHP by hydrothermal carbonization of goat bone waste for the effective adsorption of MG from aqueous solutions. Comprehensive characterization is performed using BET, FESEM, XRD, FTIR, Raman spectroscopy, and XPS to analyze the physicochemical properties of the synthesized GBHP. The effects of key experimental variables, including initial dye concentration, adsorbent dosage, solution pH, contact time, and temperature, on the results of the batch adsorption experiments were systematically analyzed. In addition, adsorption kinetics, adsorption equilibrium isotherms, thermodynamic behavior, and adsorption mechanism were fully investigated to gain detailed insight into the interaction between MG and GBHP. This study not only demonstrates the effective utilization of slaughterhouse goat bone waste as a waste-to-resource approach for sustainable management of the waste but also provides valuable insights for the development of an environmentally friendly, economically viable bio-derived adsorbent.

2. Experimental Details

2.1. Materials

Analytical-grade hydrochloric acid (HCl, 37%) and sodium hydroxide (NaOH, ≥98%) were supplied from Merck Make, India. Malachite green (MG) (analytical grade) was used as the adsorbate for the study. Aqueous solutions were obtained from reverse osmosis (RO) water produced in the laboratory. Waste goat bones (*Capra aegagrus hircus*) were collected from a local slaughterhouse in Nagpur, India. All chemicals employed during the experimental work were of analytical reagent grade (Muteeb, Ansari, et al., 2025; Waghmare et al., 2024).

2.2. Goat Bone Hydrochar

2.2.1. Pretreatment of Goat Bones

Freshly collected goat bones were manually cleaned to remove adhering muscle tissues, fat, and connective matter, followed by repeated washing under running tap water. The cleaned bones were subsequently rinsed several times with (RO) to eliminate impurities. After cleaning, the bones were air-dried at ambient laboratory conditions (25 ± 2°C) and then dehydrated in a hot-air oven at 105°C. The dried bones were crushed using a mechanical grinder and further pulverized to obtain a fine powder. The powdered material was passed through a 100-mesh sieve to ensure uniform particle size. Finally, the sieved powder was washed once again with RO water to remove loosely attached fine particles and dried at 105°C before further processing (Muteeb, Ansari, et al., 2025).

2.2.2. Chemical Activation

To enhance the physicochemical properties of the bone powder, an acid-activation treatment was performed. Approximately 25 g of the prepared goat bone powder was mixed with 100 mL of 0.6 M hydrochloric acid and stirred continuously for 1 h at room temperature using a magnetic stirrer. Acid treatment promotes the removal of inorganic impurities and improves the accessibility of surface-active sites that participate in adsorption. After activation, the suspension was separated by vacuum filtration through Whatman No. 41 filter paper. The collected solid was repeatedly washed with reverse osmosis water until the washings attained a neutral pH, indicating complete removal of residual acid. The neutralized sample was then dried in a laboratory oven at 105°C for 4 h. The obtained material was designated as activated goat bone powder (AGBP). Hydrochar was synthesized from the activated goat bone powder using a hydrothermal carbonization process. The sealed reactor was heated at 200°C for 8 h in a laboratory oven. The washed product was dried in a hot-air oven at 105°C for 24 h and subsequently stored in a desiccator to prevent moisture uptake. After acid activation and neutralization, 25 g of activated goat-bone powder (AGBP**)** was dispersed in 100 mL of distilled water, corresponding to a solid-to-liquid ratio of 1:4 (w/v). The suspension was transferred into a 200 mL Teflon-lined stainless-steel hydrothermal reactor, corresponding to approximately 50% reactor filling. The sealed reactor was heated at 200°C for 8 h under autogenous pressure. After cooling to room temperature, the hydrochar was recovered by vacuum filtration, washed repeatedly with RO water until neutral pH (~7), dried at 105°C for 24 h, and stored in a desiccator. The resulting material was designated as goat bone hydrochar powder (GBHP). The final adsorbent obtained from this procedure was referred to as GBHP for all characterization and further experiments (Waghmare et al., 2023).

2.3. Material Characterization

Synthesized Goat bone hydrochar powder (GBHP) was characterized to determine its physicochemical properties. The concentration of malachite green (MG) was determined by UV spectrophotometer (HACH DR 6000). X-ray diffraction (XRD) was used to analyze the crystalline structure of the material over a 2θ range of 10–80°, and Fourier transform infrared spectroscopy (FTIR, PerkinElmer) was used to identify the surface functional groups. The elemental composition and surface morphology of the samples were studied by field-emission scanning electron microscopy with energy-dispersive X-ray spectroscopy (FESEM–EDS, JEOL JSM-7610F). Brunauer–Emmett–Teller (BET) analysis was used to determine the specific surface area, pore volume, and pore-size distribution from N_2 adsorption–desorption isotherms. Surface chemical composition was analyzed by X-ray photoelectron spectroscopy (XPS, PHI Versa Probe III). In contrast, the structural order and graphitic nature of the hydrochar were analyzed by Raman spectroscopy (HORIBA Lab RAM HR Evolution).

2.4. Adsorption Studies

The adsorption capability of synthesized goat bone hydrochar powder (GBHP) for the removal of malachite green (MG) from aqueous media was systematically evaluated through batch adsorption experiments. The influence of operating parameters, including initial dye concentration, adsorbent dosage, solution pH, contact time, and temperature, was systematically investigated. Adsorption kinetics, equilibrium isotherms, and thermodynamic behavior were subsequently analyzed under the optimized experimental conditions. To examine the effect of initial dye concentration, 100 mL of MG solution at concentrations ranging from 10 to 60 mg L^{-1} was transferred into separate 250 mL beakers, and 0.2 g of GBHP was added to each solution. The solution pH was maintained at the desired value throughout the experiment, and the adsorption capacity and removal efficiency were calculated using the equations presented in Table 1 (Waghmare et al., 2024). The optimum adsorbent dosage was determined by varying the amount of GBHP from 0.1 to 1.5 g while maintaining the dye concentration at 60 mg L^{-1} in 100 mL of solution. The effect of pH was evaluated over the range of 2–8, whereas the contact time was varied from 10 to 90 min to determine the adsorption equilibrium time. Temperature-dependent adsorption experiments were performed between 25 and 40°C. After each adsorption experiment, the suspension was separated by filtration using Whatman No. 41 filter paper, and the residual malachite green concentration in the filtrate was determined using a UV–Visible spectrophotometer (HACH DR 6000) at the maximum absorption wavelength (Morris et al., 2024).

Table 1. Equations used for adsorption capacity, isotherm, kinetic, and thermodynamic analyses

A. EQUILIBRIUM AND CAPACITY EVALUATION

Symbol	Description	Units	Formula / Expression
C_i	Initial concentration of dye	mg L^{-1}	–
C_e	Equilibrium concentration of dye	mg L^{-1}	–
V	Volume of solution	L	–
m	Mass of adsorbent	g	–
q_e	Amount of dye adsorbed at equilibrium	mg g^{-1}	$q_e = \frac{(C_i - C_e)\,V}{m}$
Removal (%)	Percent removal of dye	%	Removal = $\frac{C_i - C_e}{C_i} \times 100$

B. ADSORPTION ISOTHERM MODELS

Model	Linear Form	Parameters and Description
Langmuir	$\frac{C_e}{q_e} = \frac{1}{q_m K_L} + \frac{C_e}{q_m}$	q_m : Maximum monolayer capacity (mg g^{-1}) K_L : Langmuir constant (L mg^{-1})
Freundlich	$\ln q_e = \ln K_F + \frac{1}{n} \ln C_e$	K_F : Freundlich constant [(mg g^{-1})(L mg^{-1})$^{1/n}$] n : Heterogeneity factor
Temkin	$q_e = B \ln A_T + B \ln C_e$	$B = \frac{RT}{b}$ (J mol^{-1}) A_T : Temkin constant (L g^{-1})

C. KINETIC MODELS

Pseudo–First–Order (PFO)

Equation	Linear Form
$\frac{dq_t}{dt} = k_1 (q_e - q_t)$	$\ln (q_e - q_t) = \ln q_e - k_1 t$

k_1 : Rate constant of PFO (min^{-1}) q_t : Amount adsorbed at time t (mg g^{-1})

Pseudo–Second–Order (PSO)

Equation	Linear Form
$\frac{dq_t}{dt} = k_2 (q_e - q_t)^2$	$\frac{t}{q_t} = \frac{1}{k_2 q_e^2} + \frac{t}{q_e}$

k_2 : Rate constant of PSO (g mg^{-1} min^{-1})

D. THERMODYNAMIC PARAMETERS

Thermodynamic Equations

Parameter	Expression	Units	Meaning
$\Delta G°$	$\Delta G° = -RT \ln K_c$	kJ mol^{-1}	Gibbs free energy
$\Delta H°$	$\ln K_c = \left(\frac{\Delta S°}{R}\right) - \left(\frac{\Delta H°}{RT}\right)$	kJ mol^{-1}	Enthalpy change
$\Delta S°$	(From intercept)	J mol^{-1} K^{-1}	Entropy change
K_c	$\frac{q_e}{C_e}$	–	Equilibrium constant
R	8.314	J mol^{-1} K^{-1}	Gas constant
T	Temperature	K	Absolute temperature

Van 't Hoff Plot

$$\ln K_c = -\frac{\Delta H°}{RT} + \frac{\Delta S°}{R}$$

Slope = $-\frac{\Delta H°}{R}$

Intercept = $\frac{\Delta S°}{R}$

C_i : Initial concentration (mg L^{-1}) C_e : Equilibrium concentration (mg L^{-1})
q_e : Amount adsorbed at equilibrium (mg g^{-1}) q_t : Amount adsorbed at time t (mg g^{-1})
x : Amount adsorbed (mg g^{-1}) t : Contact time (min) V : Volume of solution (L)
m : Mass of adsorbent (g)

3. Results and Discussion

3.1. Structural Features of GBHP

The physicochemical properties of the GBHP synthesized were examined using N_2 adsorption–desorption analysis, X-ray diffraction (XRD), Fourier transform infrared spectroscopy (FTIR), Raman spectroscopy, and X-ray photoelectron spectroscopy (XPS), as shown in Figures 1(a–f). These analyses were used to interpret the textural properties, crystalline structure, surface chemistry, graphitic characteristics, and elemental composition of the synthesized adsorbent, which are closely related to its adsorption behavior for malachite green (MG).

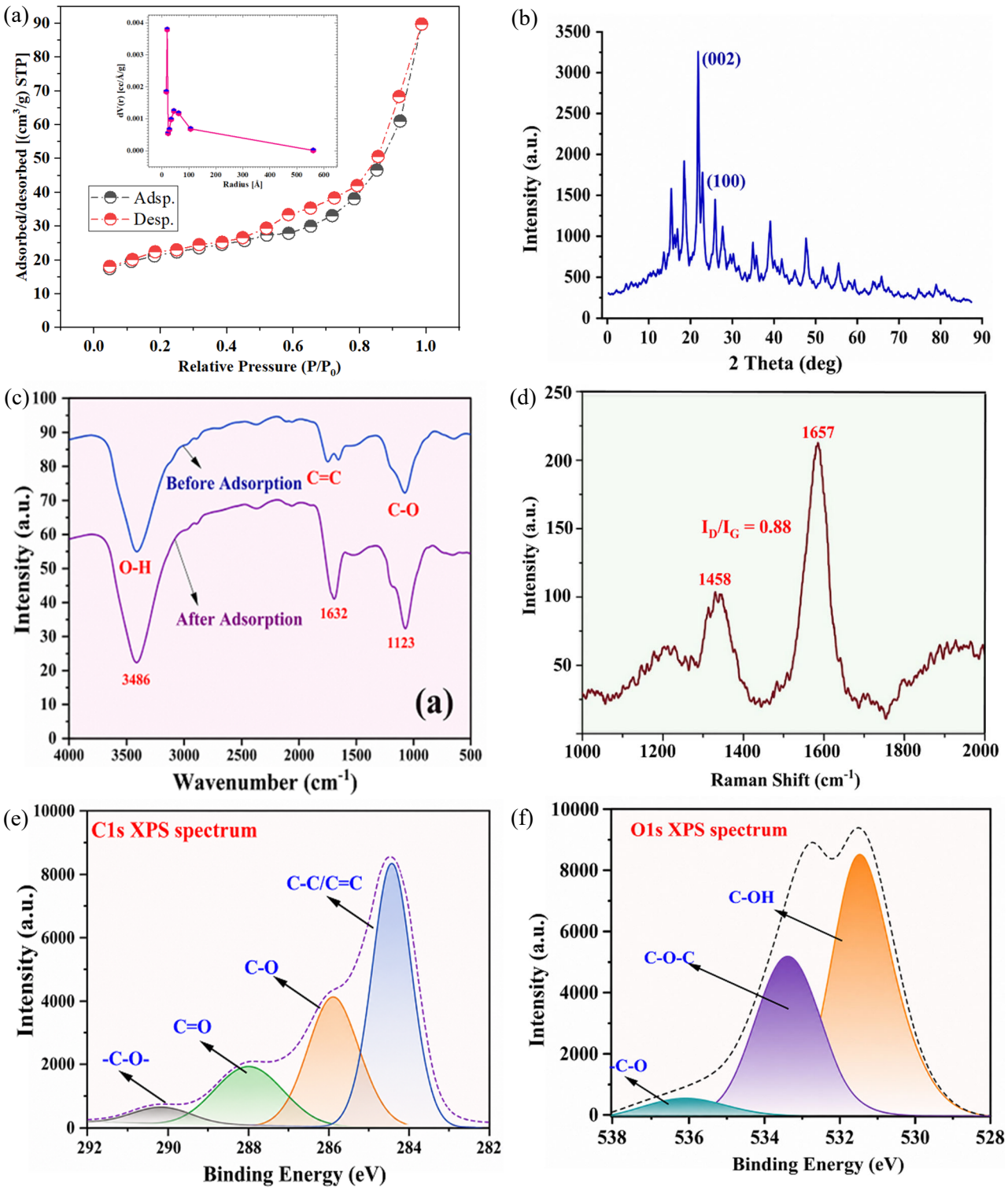

Fig. 1. Structural features of GBHP: (a) BET isotherm and pore statistics, (b) XRD pattern, (c) FTIR spectra, (d) Raman spectrum, (e) C1s XPS, and (f) O1s XPS spectra

The N_2 adsorption–desorption isotherm shown in Figure 1(a) exhibits a typical hysteresis loop at high pressure ($P/P_0 > 0.8$), characteristic of mesoporous structures. Nitrogen uptake increases gradually and is sharply increased near the saturation pressure, indicating multilayer adsorption and capillary condensation within interconnected mesopores. The synthesized GBHP had a BET surface area of ~16.8 $m^2 g^{-1}$, a total pore volume of 0.139 $cm^3 g^{-1}$, and an average pore diameter of 4.6 nm, indicating the formation of a mesoporous carbon framework. The pore-size distribution also showed that the pores are mainly in the mesoporous region, which promotes the diffusion of malachite green molecules and reduces diffusion resistance within the particles. Pore development is believed to result from reactions during hydrothermal carbonization, including dehydration, decarboxylation, and volatilization, which create interconnected pore channels and expose additional adsorption sites. The XRD pattern of GBHP, shown in Figure 1(b), shows peaks at 24° and 43°, which are associated with the (002) and (100) planes of graphitic carbon, respectively. The general diffraction peak shape suggests a lack of graphitic order with a mostly turbostratic carbon structure, typical of hydrothermally carbonized biomass. The lack of sharp graphitic reflections indicates that complete graphitization has not taken place under the conditions applied here, and the defect-rich amorphous carbon matrix has been preserved. In addition, there are some weak diffraction peaks seen across the diffractogram, which belong to the phases of calcium phosphate and hydroxyapatite from the goat bone precursor.

The presence of both partially graphitized carbon and remnant mineral phases creates a variety of adsorption sites, which might synergistically increase the adsorption of malachite green via both electrostatic and surface complexation processes. The FTIR spectra before and after adsorption, as shown in Figure 1(c), indicate that the GBHP surface contains numerous oxygen-containing functional groups. The wide absorption band at 3486 cm^{-1} is attributed to the stretching of hydroxyl (–OH) groups, and the absorption band at 1632 cm^{-1} is attributed to the aromatic C=C stretching vibrations formed during the hydrothermal carbonization process. The band at 1123 cm^{-1} is due to C–O stretching vibrations of alcohol, ether, and phenolic groups. After malachite green adsorption, there was a significant drop in the peak intensity and a slight shift in the bands, indicating that the functional groups were directly involved in the adsorption process. The spectral shifts indicate that hydrogen bonding, electrostatic attraction, and a π–π electron donor–acceptor interaction between the aromatic ring of malachite green and the conjugated carbon of GBHP are involved in the adsorption process.

The Raman spectrum shown in Figure 1(d) features the characteristic D and G bands at 1458 and 1657 cm^{-1}, respectively. The ratio of the D band to G band intensities ($I_D/I_G = 0.88$) indicates a medium degree of defectiveness in the carbon structure, with partially formed graphitic domains. The defect generation during HC is relatively high, which is advantageous for adsorption, as defect sites have higher surface energy and hence more chemically active sites available for dye adsorption. At the same time, the graphitic domains enable π–π stacking interactions with the aromatic structure of malachite green, thereby improving adsorption affinity (Durak et al., 2026; Hart et al., 2023).

The XPS spectra shown in Figure 1(e–f) also indicate the heterogeneous surface chemistry of GBHP. The deconvoluted C1s spectrum consists of four components that are centered at approximately 284.5, 286.0, 288.1, and 290.2 eV, which can be assigned to C–C/C=C, C–O, C=O, and O–C=O species, respectively. Similarly, the O 1s spectrum can be resolved into three oxygen environments centered near 531.5 eV, 533.2 eV, and 535.6 eV, corresponding to C–OH, C–O–C, and oxygen-rich carbonyl or adsorbed oxygen species, respectively. The preference for graphitic carbon over other carbon forms, along with the presence of a significant number of oxygen-containing functional groups, confirms the successful hydrothermal carbonization, creating a chemically heterogeneous surface that interacts with malachite green through multiple adsorption mechanisms (Beulah & Muthukumaran, 2020; Inala & Choksi, 2025). The presence of oxygenated active groups increases the site's polarity. It provides hydrogen bonding and electrostatic attraction, as well as the aromatic carbon framework for strong π–π interactions with the dye molecules. The physicochemical characterization results overall show that the hydrothermal carbonization process successfully converted goat bone waste into a mesoporous carbonaceous adsorbent with a defect-rich, partially graphitized structure, containing high levels of oxygen-containing functional groups and some mineral phases remaining. All these structural and surface properties combine to enhance the adsorption capacity of the GBHP by providing conditions that promote molecular diffusion and multiple interactions with malachite green molecules (Arunprasath et al., 2019).

3.2. Surface Morphological Analysis (FESEM)

The surface characterization of the synthesized GBHP onto MG adsorption was analyzed using Field Emission Scanning Electron Microscopy (FESEM) coupled with three-dimensional (3D) surface topography, as presented in Figures 2(a–d). The pristine GBHP, as shown in Figure 2(a), displays a heterogeneous, well-developed porous carbonaceous framework characterized by interconnected pores, voids, and a fractured morphology. The morphological features highlight the successful formation of a porous framework with ample

accessible adsorption sites and good diffusion of MG molecules into the internal pore structure. The 3D surface profile shown in Figure 2(b) also shows clear peaks, valleys, and irregularities, indicating a rough, uneven terrain. The surface morphology changes considerably after adsorption, as shown in Figure 2(c), with the surface partially filled by the MG molecules, making it denser and more compact. The decrease in the visible pore volume and the surface voids indicate successful pore filling and adsorption of dye molecules in the porous matrix, as shown in Figure 2(d).

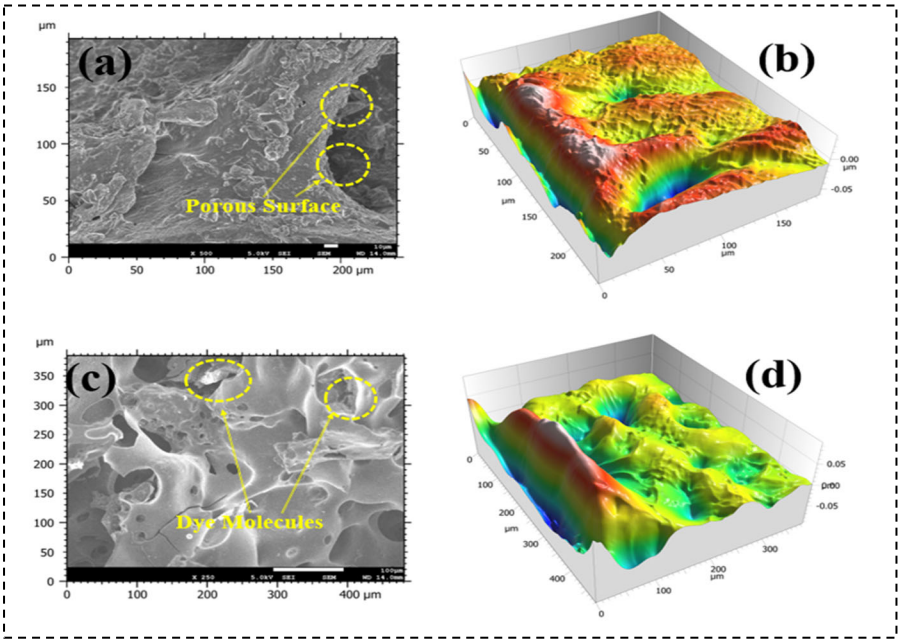

Fig. 2. FESEM and 3D surface morphology of GBHP: (a, b) before adsorption and (c, d) after MG adsorption

The morphological transformation observed is consistent with the BET analysis, which showed that the material is mesoporous, and with the FTIR and XPS results, which confirmed the presence of abundant oxygen-containing functional groups. The results indicate that the adsorption of MG onto GBHP is controlled by a synergistic process in which the mechanisms of pore filling, electrostatic attraction, hydrogen bonding, π–π electron donor–acceptor interactions between the aromatic structure of MG and the partially graphitized carbon matrix, as well as adsorption by surface complexation through hydroxyl and carbonyl functionalities, all participate. Thus, FESEM and 3D topographical analysis can be used to provide direct morphological evidence of the high adsorption ability of GBHP towards malachite green.

3.3. Adsorption Optimization Studies

The adsorption behavior of goat bone hydrochar powder (GBHP) toward malachite green (MG) has been systematically evaluated by studying various parameters such as dye concentration, adsorbent dosage, pH, contact time, and temperature, as depicted in Figures 3(a–e). The adsorption capacity (q_e) and the removal efficiency (R%) were determined using the equations listed in Table 1. Optimization of these operating parameters is crucial to maximize dye removal by enhancing mass-transfer efficiency and increasing the accessibility of surface sites. As a result, the adsorption efficiency rose rapidly with increasing MG concentration in the range of 5–20 mg L^{-1}, as shown in Figure 3(a), and then slowly to about 90% at 40 mg L^{-1}. Further increases in concentration did not yield a significant increase in adsorption, indicating progressive saturation of the available adsorption sites. The initial rise is explained by the high concentration difference between the solution and the adsorbent surface, which increases the mass transfer of MG molecules to a high level, resulting in the achievement of adsorption equilibrium.

The dosage of adsorbent, as illustrated in Figure 3(b), showed that the elimination efficiency increased from about 70% to 93% as the loading of GBHP increased from 0.1 to 1.5 g. This behavior accelerates the formation of higher numbers of surface-functional sites and oxygenated functional groups involved in adsorption. But increasing the dosage only slightly improved the removal efficiency, indicating that adsorbent particles may aggregate and that adsorption sites may overlap, resulting in a reduced effective surface area. The effects of solution pH, as illustrated in Figure 3(c), revealed that solution pH significantly influenced adsorption behavior, and the surface charge of GBHP was found to be crucial. The removal efficiency increased from about 80% at pH 2 to 96% at pH 6, then decreased slightly in the alkaline pH range. Lower pH results in proton

enrichment at the GBHP surface, with H+ ions and positively charged MG molecules. At a lower pH, nearly neutral, deprotonation of the oxygen-containing functional groups on the GBHP surface increased the density of negatively charged adsorption sites, thereby strengthening electrostatic interactions with cationic MG molecules and enhancing overall adsorption efficiency. The adsorption kinetics shown in Figure 3(d) suggest that adsorption occurred in two stages: a fast initial stage of dye removal during the first 30 min and a slower stage approaching equilibrium after about 90 min, where equilibrium removal reached ~92%. The rapid initial adsorption was due to the abundance of energetically favorable binding sites on the GBHP surface, whereas the subsequent slower phase was due to intraparticle diffusion and the gradual filling of the remaining active sites in the GBHP until reaching dynamic equilibrium.

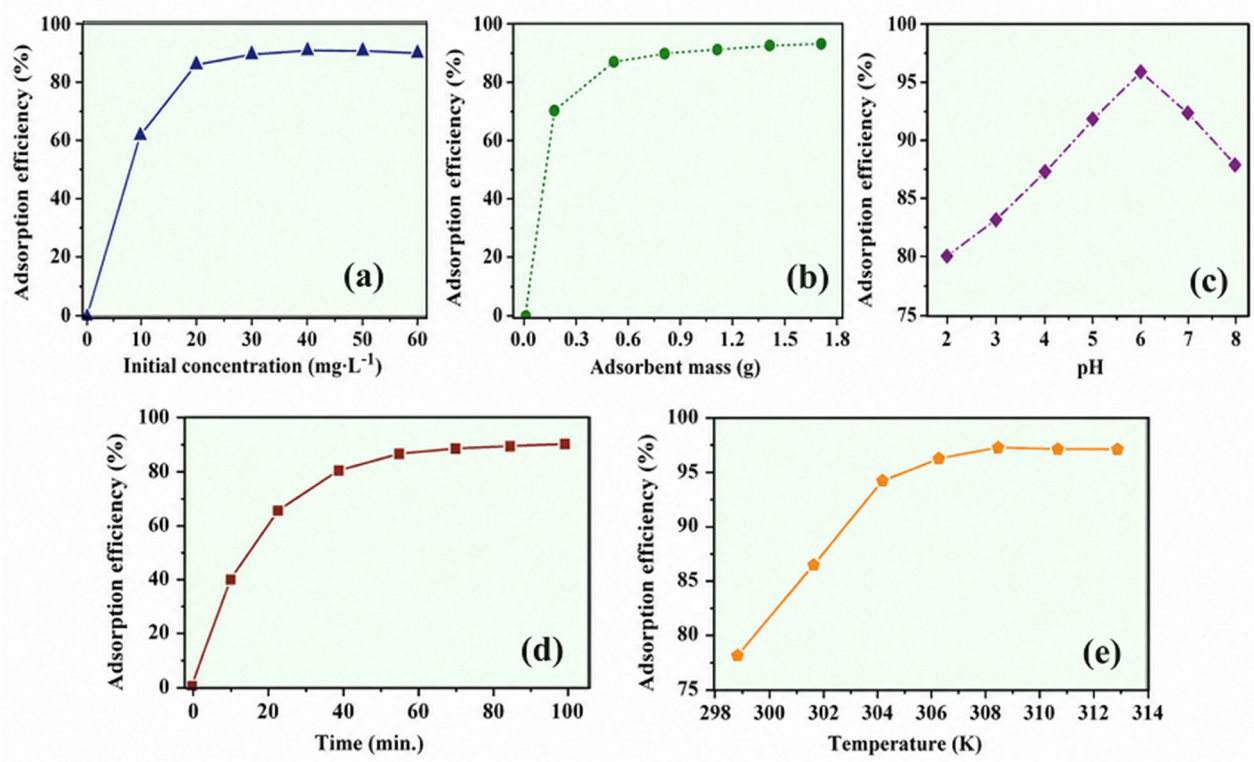

Fig. 3. Effect of operating parameters on MG adsorption by GBHP: (a) initial dye concentration, (b) adsorbent dosage, (c) solution pH, (d) contact time, and (e) temperature

The effect of temperature, as illustrated in Figure 3(e), indicated that the efficiency of the adsorption increased from about 78% at 298K to 97% at 308K and remained almost unchanged till 313K. It is seen that the adsorption at higher temperatures is higher, which suggests endothermic adsorption of MG on the GBHP. As the temperature rises, the diffusion resistance decreases and molecular mobility increases, promoting the diffusion of dye molecules into the inner pore structure of the adsorbent material. From the results of adsorption optimization, GBHP shows excellent adsorption capacity for MG at an initial dye concentration of 40 mg L^{-1}, adsorbent dosage of 1.5 g, pH 6, contact time of 90 min, and temperature of 308K. These optimized conditions were then used for the adsorption isotherm, kinetic, and thermodynamic studies.

3.4. Kinetics Modeling

The kinetic study of the adsorption of malachite green MG on GBHP was calculated using pseudo-first-order (PFO) and pseudo-second-order (PSO) models, as depicted in Figures 4(a–b). The linear equations corresponding to each are listed in Table 1. Adsorption kinetic models were employed to identify the controlling step of the adsorption process and clarify whether physical or chemical interactions govern MG uptake. The model plot for PFO, shown in Figure 4(a), represents the variation of $\log(q_e - q_t)$ as a function of contact time. The correlation coefficient for the obtained data was relatively low ($R^2 = 0.71$), indicating that the PFO model was not suitable for modeling MG adsorption on GBHP. The poor fit indicates that the adsorption process does not follow simple diffusion and that the adsorption site is not a uniform surface. The experimental points deviate further from the fitted line, suggesting that the rate of adsorption is not solely dependent on the concentration of unoccupied adsorption sites. However, the PSO model in Figure 4(b) illustrates a very good linear relationship between t/q_t and time, with a very high correlation coefficient ($R^2 = 0.99$). The high value of this

agreement indicates that the pseudo-second-order kinetic model was followed for the adsorption of MG onto GBHP. The result indicates that the adsorption rate is primarily dependent on surface-active sites and chemisorption-type interactions, such as electron sharing, electrostatic attraction, hydrogen bonding, and π–π interactions, between MG molecules and the functionalized carbon surface of GBHP.

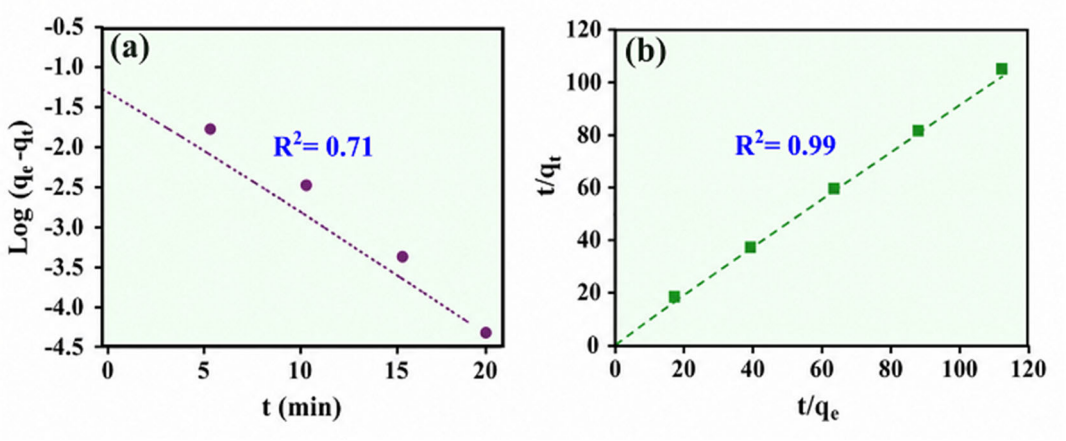

Fig. 4. Adsorption kinetic models for MG adsorption onto GBHP: (a) PFO and (b) PSO

Compared with both models, the PSO model exhibits superior performance because chemical interactions, which play a dominant role in the adsorption of MG onto GBHP, are not only due to simple mass transfer but also to a specific site adsorption mechanism, as shown in Table 2. This behavior is in line with the FTIR and XPS results, which confirmed the presence of hydroxyl, carbonyl, and C–O groups that interact with the MG molecules. Therefore, the kinetic results confirm that the adsorption sites of GBHP are chemically active, and that the removal of MG is primarily surface-controlled, with a considerable contribution from chemisorption.

Table 2. Kinetic parameters for MG adsorption onto GBHP

Kinetic Model	Parameters	Value
Pseudo-First Order (PFO)	Linear equation	y = −0.0023x − 1.315
	R^2	0.71
	k_1 (min^{-1})	0.0063
	qecal (mg/g)	0.246
Pseudo-Second Order (PSO)	Linear equation	y = 0.3028x + 0.2394
	R^2	0.9901
	qecal (mg/g)	3.23
	k_2 (g mg^{-1} min^{-1})	0.152

3.5. Adsorption Isotherms

The equilibrium adsorption behavior of malachite green (MG) onto goat bone hydrochar powder (GBHP) was investigated using the Langmuir, Freundlich, and Temkin isotherm models, are presented in Table 1. At the same time, the corresponding fitting plots are illustrated in Figures 5(a–d). Isotherm analysis provides valuable information on the adsorption mechanism, surface heterogeneity, adsorption capacity, and adsorbate–adsorbent interactions at equilibrium. The linear Langmuir plot in Figure 5(a), exhibited an excellent correlation coefficient (R^2 = 0.9504) with the regression equation $1/q_e = 4.7232(1/C_e) + 6.8197$, indicating that the adsorption of MG is reasonably described by monolayer adsorption on energetically equivalent adsorption sites. The satisfactory fitting suggests that each adsorption site accommodates one dye molecule without significant interaction between adjacent adsorbed species. The best-fit Langmuir model further confirms that the oxygen-containing functional groups and defect sites identified by FTIR, Raman, and XPS analyses serve as the primary adsorption centers responsible for MG uptake.

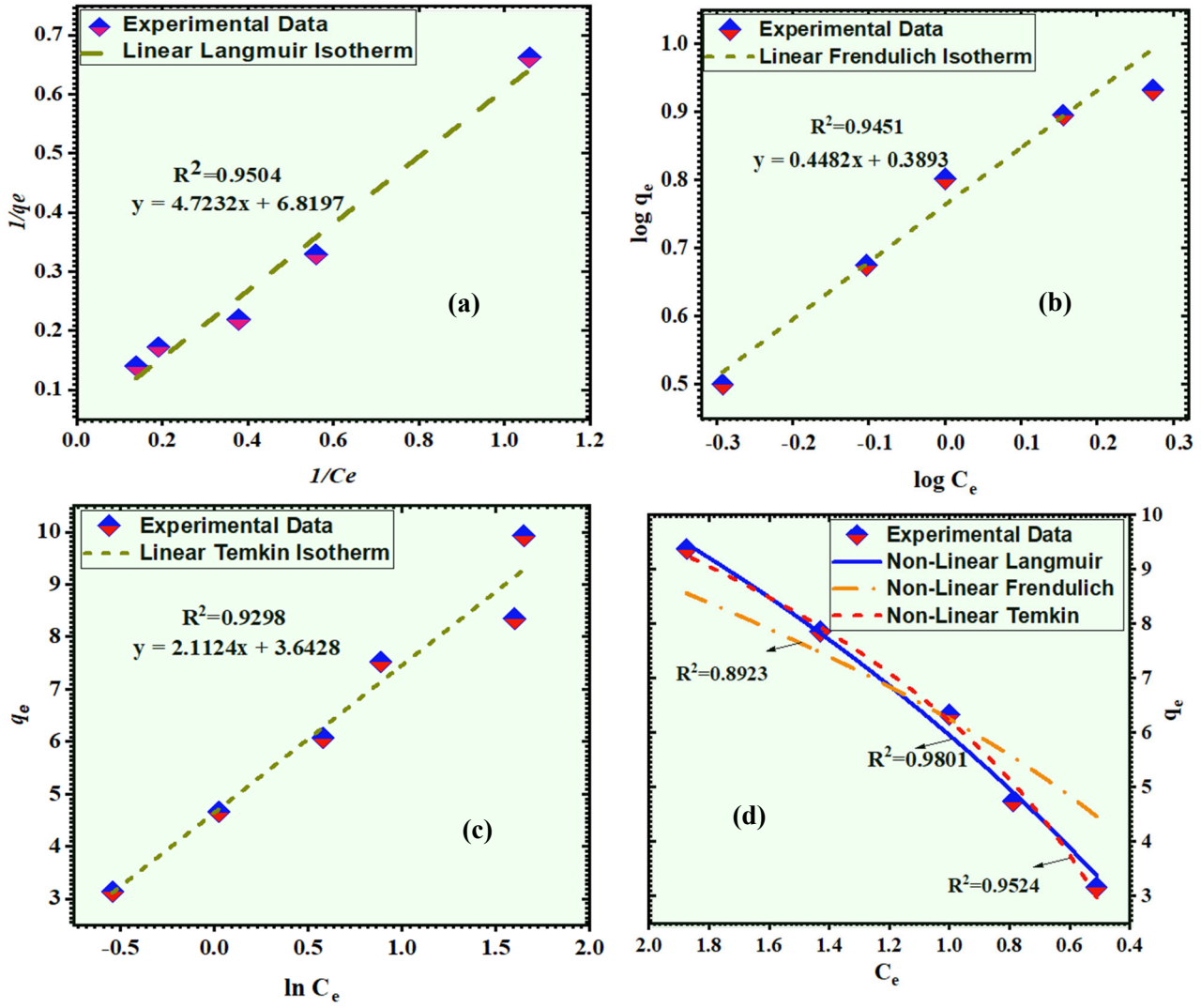

Fig. 5. Adsorption isotherm models for MG adsorption onto GBHP: (a) Langmuir, (b) Freundlich, (c) Temkin, and (d) nonlinear isotherm fitting

The Freundlich isotherm, as illustrated in Figure 5(b), showed a good fit ($R^2 = 0.9451$) with the regression equation $\log q_e = 0.4482 \log C_e + 0.3893$, indicating that GBHP possesses a moderately heterogeneous surface. The slightly lower correlation coefficient compared with the Langmuir model suggests that although surface heterogeneity exists, monolayer adsorption remains the dominant equilibrium mechanism. The Freundlich behavior reflects the existence of adsorption sites possessing different surface energies arising from the coexistence of graphitic carbon, hydroxyl groups, carbonyl groups, and residual mineral phases within the hydrochar matrix. The Temkin model, as shown in Figure 5(c), provides a linear correlation among the three linear isotherms with $R^2 = 0.9298$, with the regression equation $q_e = 2.1124 \ln C_e + 3.6428$. The results indicate a progressive decline in adsorption energy as surface occupancy increases, owing to interactions between adsorbed MG molecules and the GBHP surface during adsorption. The applicability of the Temkin model suggests that electrostatic attraction, hydrogen bonding, π–π interactions, and surface complexation collectively contribute to MG adsorption rather than a purely physical adsorption mechanism.

To further evaluate the adsorption behavior, nonlinear fitting was performed using the Langmuir, Freundlich, and Temkin equations as in Figure 5(d). Among the nonlinear models, the Langmuir model exhibited the best fitting ($R^2 = 0.9801$), followed by the Freundlich ($R^2 = 0.9524$) and Temkin ($R^2 = 0.8923$) models. The superior nonlinear Langmuir fitting confirms that monolayer adsorption predominates on the GBHP surface and validates the assumptions of the linear Langmuir analysis. The relatively lower fitting achieved with the Freundlich and Temkin models indicates that surface heterogeneity and variations in adsorption energy influence MG uptake; however, these effects are secondary to the predominant monolayer adsorption mechanism.

Overall, both linear and nonlinear isotherm analyses demonstrate that malachite green adsorption onto GBHP is predominantly governed by Langmuir-type monolayer adsorption, with additional contributions from heterogeneous surface interactions described by the Freundlich and Temkin models. The excellent agreement of the Langmuir model indicates that the synthesized GBHP possesses uniformly distributed active adsorption sites capable of efficiently adsorbing MG molecules, while the oxygen-containing functional groups and defect-rich carbon framework facilitate strong adsorbate–adsorbent interactions under equilibrium conditions (Kizilkaya, 2012).

3.6. Thermodynamic Study

The thermodynamic parameters of adsorption of MG on GBHP were studied at different temperatures (293, 298, 303, and 308 K), and the results are given in Table 3. Estimations of thermodynamic parameters were carried out using the relationships summarized in Table 1, and the good linearity of the Van't Hoff plot shown in Figure 6 ($R^2 = 0.9899$) indicates that the adsorption equilibrium in the studied temperature range exhibits classical thermodynamic behavior. The calculated Gibbs free energy (ΔG°) values were −2.690, −2.677, −2.664, and −2.651 kJ mol^{-1} at 293, 298, 303, and 308 K, respectively. Negative ΔG° values indicate that the adsorption of MG on GBHP is spontaneous over the studied temperature range. In addition, the relatively small value of ΔG° (around -2 kJ mol^{-1}) confirms adsorption via physisorption and weak chemisorption interactions, rather than purely chemical bonding. The gradual reduction in the magnitude of ΔG° with increasing temperature suggests that adsorption becomes progressively weaker, indicating that the affinity of the MG molecules for the GBHP surface is greater at lower temperatures. The exothermic nature of MG adsorption was verified by the negative ΔH° value of (-3.451 kJ mol^{-1}), which means that heat is released as MG molecules become immobilized on the active sites of GBHP (Gumus et al., 2012). The magnitude of ΔH° falls within the range usually observed for adsorption processes, including both physical and specific surface adsorption, suggesting that several adsorptive mechanisms may be involved simultaneously in the removal of MG. The exothermic nature indicates that after adsorption of MG molecules on the active sites, the adsorbent–adsorbate interactions become energetically stable without the need for further thermal energy. The electrostatic attraction, hydrogen bonding, and π–π electron donor–acceptor interaction between the aromatic rings of MG and the partially graphitized carbon framework, in addition to surface complexation involving OH, CO, and ether functional groups, as revealed by FTIR and XPS studies, may govern these interactions.

The value of the entropy change (ΔS° = −0.002598 kJ mol^{-1} K^{-1}) was also found to be negative, indicating that the degree of disorder at the solid solution interface decreases as adsorption progresses. This decrease in entropy indicates that, upon immobilization on the GBHP surface, the MG molecules adopt a more aligned configuration than the freely moving molecules in the aqueous phase, replacing the less orderly aqueous-phase molecules with a more orderly adsorbed layer. The negative entropy change is also attributed to the establishment of stable adsorbate–adsorbent interactions and suggests a decrease in configurational freedom at equilibrium.

Table 3. Thermodynamic parameters for MG adsorption onto GBHP

Temperature (Kelvin)	Thermodynamic Parameters			
	ΔG^0(kJmol^{-1})	ΔH^0(kJmol^{-1})	ΔS^0(kJmol^{-1}K^{-1})	R^2
293	-2.690	-3.451	- 0.002598	0.9899
298	-2.677			
303	-2.664			
308	-2.651			

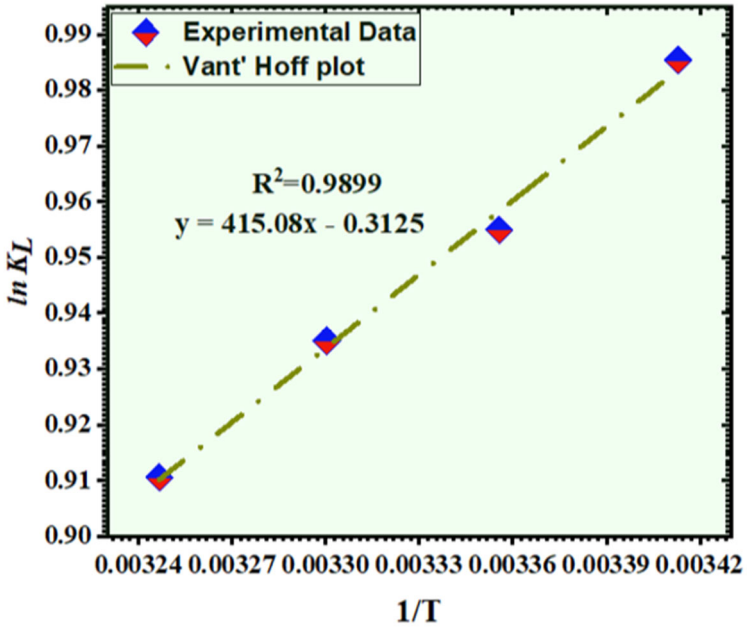

Fig. 6. Van't Hoff analysis of GBHP

4. Adsorption Mechanism

The proposed adsorption mechanism of MG on GBHP is shown in Figure 7.

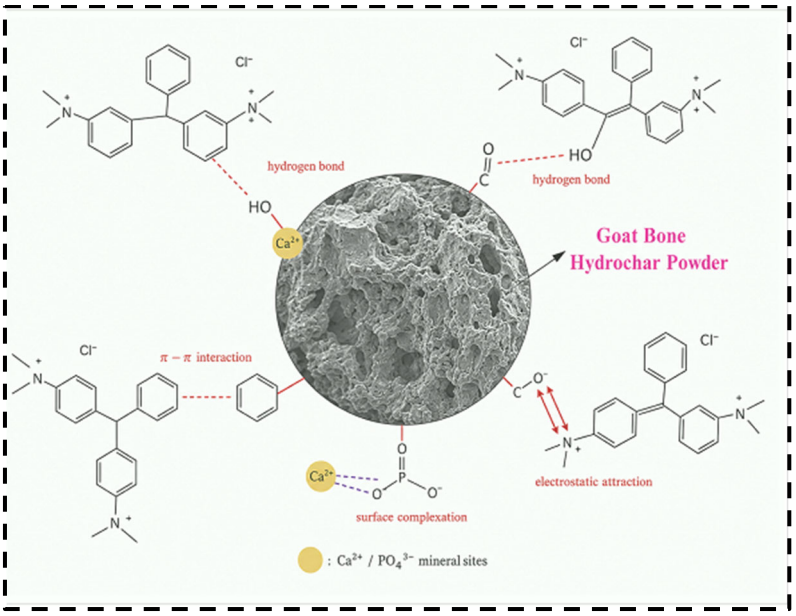

Fig. 7. Proposed adsorption mechanism of malachite green onto goat bone hydrochar powder (GBHP)

The removal process is driven by the synergistic effects of various physicochemical interactions related to the porous carbonaceous structure, O-containing surface functionalities, and naturally occurring mineral components in GBHP. At first, the MG molecules migrate across the liquid boundary layer before reaching the external surface of GBHP, then into the interconnected pore network. The BET and FESEM analysis show that the mesoporous structure is well formed, with many accessible adsorption sites, which also help fill the pores, resulting in efficient diffusion and the confinement of MG molecules within the internal porous structure. The abundance of oxygen-containing functional groups, such as hydroxyl (–OH), carbonyl (C=O), carboxyl (–COOH), and ether (C–O) groups, created during hydrothermal carbonization further promotes adsorption. These functional groups are active adsorption centers that can form hydrogen bonds with the nitrogen-containing functional groups of malachite green, thereby enhancing adsorbate–adsorbent interaction. At the same time, partial deprotonation of these oxygenated groups at the optimal adsorption pH creates

negatively charged surface sites that strongly attract the positively charged MG molecules. The partially graphitized carbon framework, detected by XRD and Raman analysis, is also an important feature in the adsorption process (Khan M.I. et al., 2025). The aromatic carbon structure of GBHP provides electron-rich sites capable of interacting with the aromatic surface of MG through π–π interactions contained in GBHP. In addition, the presence of mineral species in the residual matter from the goat bone compound, such as calcium and phosphate, can be coordinated with the oxygen-containing surface groups of the dye molecules, which increases the affinity for the adsorption of the dye molecules on the surface (Arshad et al., 2026; Singh et al., 2025). The presence of these adsorption pathways also suggests that the removal of MG using GBHP is not dominated by a single interaction mechanism, but rather by a combination of pore filling, hydrogen bonding, electrostatic attraction, π–π interactions, and surface complexation. The synergistic adsorption mechanism is in line with the PSO kinetic model and the Langmuir adsorption isotherm, as well as the FTIR and XPS results, which indicate that both the porous structure and surface chemical functionalization contribute to the high adsorption capacity of GBHP for MG.

5. Conclusion

In this study, the effective conversion of waste goat bones to sustainable goat bone hydrochar powder (GBHP) by hydrothermal carbonization was performed for the removal of MG from an aqueous solution. Physicochemical characterization confirmed that the carbonaceous structure formed had a mesoporous structure with defects, a BET surface area of 16.8 $m^2\ g^{-1}$, a pore volume of 0.139 $cm^3\ g^{-1}$, and an average pore diameter of 4.6 nm. XRD, FTIR, Raman, and XPS analyses showed that the carbon framework was partially graphitized and contained oxygen-containing functional groups and mineral-phase impurities, which provided abundant active adsorption sites. Under optimized conditions (40 mg L^{-1} initial dye concentration, 1.5 g adsorbent dosage, pH 6, 90 min contact time, and 308 K), GBHP achieved an adsorption efficiency of about 97%. The PSO model ($R^2 = 0.9901$) showed the highest correlation with experimental results by surface interactions. The equilibrium data showed a good correlation with the Langmuir isotherm, indicating homogeneous adsorption on a single layer of MG molecules. In addition, thermodynamic investigations demonstrated that the reaction was exothermic and spontaneous, with a decrease in interfacial randomness. The adsorption mechanism proposed demonstrated that the contributions of pore filling, electrostatic attraction, hydrogen bonding, π–π interactions, and surface complexation to the removal of MG were all considered. The adsorption behavior of GBHP was assessed using laboratory-scale batch experiments; however, the results would still be beneficial and insightful for bone-derived hydrochar adsorption. The continuous flow system, regeneration and reuse systems, real industrial wastewater treatment, competitive multi-component adsorption, and techno-economic evaluation are proposed for future research, with the potential to serve as a low-cost waste-derived adsorbent for dye-contaminated wastewater.

Acknowledgements

The authors thank King Faisal University, Saudi Arabia, for providing the resources for conducting this study.

Funding Statement

This work was supported by the Deanship of Scientific Research, Vice Presidency for Graduate Studies and Scientific Research, King Faisal University, Saudi Arabia [Grant No. KFU264843].

References

Abioye, K.J., Falua, K.J., Rezaee, M., Zamiri, M.A., Zou, F., & Acharya, B. (2025). Global insights into biomass pyrolysis mechanisms: A scientometric and mechanistic approach. *Results in Engineering*, *28*, 107123. https://doi.org/https://doi.org/10.1016/j.rineng.2025.107123

Abioye, K.J., Harun, N.Y., Chofreh, A.G., Kamyab, H., Yusuf, M., Jagaba, A.H., … Ighalo, J.O. (2025). Trends and Advancements in Utilization of Biomass Waste for Gasification: A Bibliometric Review. *GCB Bioenergy*, *17*(12), e70095. https://doi.org/https://doi.org/10.1111/gcbb.70095

Abioye, K.J., Harun, N.Y., Sufian, S., Yusuf, M., Jagaba, A.H., Waqas, S., … Kang, K. (2024). Optimization of syngas production from co-gasification of palm oil decanter cake and alum sludge: An RSM approach with char characterization. *Environmental Research*, *246*, 118027. https://doi.org/https://doi.org/10.1016/j.envres.2023.118027

Abioye, K.J., Harun, N.Y., Yusuf, M., Kamyab, H., Ighalo, J.O., Almusattar, W., … Pande, S. (2024). RSM-based co-gasification of palm oil decanter cake and sugarcane bagasse: Syngas production and biochar characteristics. *Biomass and Bioenergy*, *191*, 107482. https://doi.org/https://doi.org/10.1016/j.biombioe.2024.107482

Arshad, M.S., Ansari, K., Waghmare, C., Eyvaz, M., Alqahtani, D.A., & Alkhtani, N.A.N. (2026). Thermochemical Conversion and Activation-Driven Performance of Coconut Biochar: A Critical Review on Structure–Property–Adsorption Relationships in Dye Wastewater Treatment. *International Journal of Environmental Research*, *20*(5), 250. https://doi.org/10.1007/s41742-026-01205-2

Arunprasath, T., Sudalai, S., Meenatchi, R., Jeyavishnu, K., & Arumugam, A. (2019). Biodegradation of triphenylmethane dye malachite green by a newly isolated fungus strain. *Biocatalysis and Agricultural Biotechnology*, *17*, 672–679. https://doi.org/10.1016/J.BCAB.2019.01.030

Awad, A.M., Shaikh, S.M.R., Jalab, R., Gulied, M.H., Nasser, M.S., Benamor, A., & Adham, S. (2019). Adsorption of Organic Pollutants by Natural and Modified Clays : A Comprehensive Review. *Separation and Purification Technology*, 115719. https://doi.org/10.1016/j.seppur.2019.115719

Beulah, S.S., & Muthukumaran, K. (2020). Methodologies of Removal of Dyes from Wastewater: A Review. *International Research Journal of Pure and Applied Chemistry*, 68–78. https://doi.org/10.9734/IRJPAC/2020/V21I1130225

Bian, Y., Zhang, Y., Chen, Z., Xu, L., Zhang, C., Shi, D., … Wang, X. (2025). Malachite green in environmental samples: Updates on sources, fates, distribution and removal techniques. *Ecotoxicology and Environmental Safety*, *303*, 118978. https://doi.org/10.1016/j.ecoenv.2025.118978

Boakye, P., Ohemeng-Boahen, G., Darkwah, L., Neuyam, Y. A. S., Appiah-Effah, E., Oduro-Kwarteng, S., … Woo, S. H. (2024). Waste Biomass and Biomaterials Adsorbents for Wastewater Treatment. https://doi.org/10.60692/fj7f2-vjy65

Bushra, R., Mohamad, S., Alias, Y., Jin, Y., & Ahmad, M. (2021). Current approaches and methodologies to explore the perceptive adsorption mechanism of dyes on low-cost agricultural waste: A review. *Microporous and Mesoporous Materials*, *319*(March), 111040. https://doi.org/10.1016/j.micromeso.2021.111040

Clark, T., Chandrasekhar, J., Spitznagel, G.W., & Schleyer, P.V.R. (1983). Efficient diffuse function-augmented basis sets for anion calculations. III. The 3-21+G basis set for first-row elements, Li–F. *Journal of Computational Chemistry*, *4*(3), 294–301. https://doi.org/10.1002/JCC.540040303

Durak, H., Yarbay, R.Z., & Türkmen, B.A. (2026). Hydrothermal Carbonization of Biomass for Hydrochar Production: Mechanisms, Process Parameters, and Sustainable Valorization. *Processes*. https://doi.org/10.3390/pr14020339

Gumus, R.H., Wauton, I., & Aliu, A.M. (2012). Investigation of the effect of Chemical Activation and characterization of bone char: Cow bone. *Journal of Engineering and Applied Science*, *4*, 34–45.

Hart, A., Ebiundu, K., Peretomode, E., Onyeaka, H., Nwabor, O. F., & Obileke, K. (2022). Value-added materials recovered from waste bone biomass: technologies and applications. *RSC Advances*, *12*(34), 22302–22330. https://doi.org/10.1039/d2ra03557j

Hart, A., Omonmhenle, S.I., & Peretomode, E. (2023). Waste bone char-derived adsorbents: characteristics, adsorption mechanism and model approach. *Environmental Technology Reviews*, *12*(1), 175–204. https://doi.org/10.1080/21622515.2023.2197128

He, J., Mo, P.-H., Luo, Y.-S., & Yang, P. (2023). Strategies for Solving the Issue of Malachite Green Residues in Aquatic Products: A Review. *Aquaculture Research*, *2023*, 1–17. https://doi.org/10.1155/2023/8578570

Hussain, N., Kumar, J., Ali, S., Ahmed, S., & Fatima, N. (2021). Development of fruit waste derived bio-adsorbents for wastewater treatment : A review. *Journal of Hazardous Materials*, *416*(April), 125848. https://doi.org/10.1016/j.jhazmat.2021.125848

Inala, B.V.P., & Choksi, N. (2025). Animal Bone- Eco-friendly Adsorption Material in Waste Water Treatment. *International Journal For Multidisciplinary Research*, 7(1). https://doi.org/10.36948/ijfmr.2025.v07i01.35458

Jankovská, Z., Peikertova, P., Tokarský, J., & Matejová, L. (2025). Adsorbents prepared by pyrolysis for VOC abatement. https://doi.org/10.21203/rs.3.rs-7807256/v1

Khan, A.M., Usmani, M.A., Yasmeen, K., Ahmed, M.N., Obaid, M., Naz, S.A., … Aslam, S. (2023). Conversion of waste animal bones to biofertilizer and adsorbent for wastewater treatment: An innovative approach to develop zero-waste technology. Retrieved from https://doi.org/10.21203/rs.3.rs-3134479/v1

Khan, M.I., Sufian, S., Hassan, F., Shamsuddin, R., & Farooq, M. (2025). Phosphoric acid based geopolymer foam-activated carbon composite for methylene blue adsorption: isotherm, kinetics, thermodynamics, and machine learning studies. *RSC Advances*, *15*(3), 1989–2010. https://doi.org/https://doi.org/10.1039/d4ra05782a

Kizilkaya, B. (2012). Usage of biogenic apatite (fish bones) on removal of basic fuchsin dye from aqueous solution. *Journal of Dispersion Science and Technology*, *33*(11), 1596–1602.

Kumar, A., Devnani, G.L., & Pal, D.B. (2025). Sustainable Degradation of Organic Pollutants Using Various Treatment Processes: A Review. https://doi.org/10.69709/susproc.2025.111130

Ledakowicz, S., & Paździor, K. (2021). Recent Achievements in Dyes Removal Focused on Advanced Oxidation Processes Integrated with Biological Methods. *Molecules*, *26*(4), 870. https://doi.org/10.3390/MOLECULES26040870

Li, Y., Wang, M., Shan, Y., Liu, J., Han, L., & Liu, X. (2024). Adsorption characteristics and molecular mechanisms of ionic organic pollutants on bone char. *Journal of Molecular Liquids*, 400, 124624.

Limeneh, D.Y., Tesfaye, T., Ayele, M., Husien, N.M., Ferede, E., Haile, A., … Kong, F. (2022). A Comprehensive Review on Utilization of Slaughterhouse By-Product: Current Status and Prospect. *Sustainability*, *14*(11), 6469. https://doi.org/10.3390/su14116469

Morris, A.R., Patil, A.J., Sadekar, S., Choudhury, A., Munde, M., Chougale, A.D., … Dawkar, V.V. (2024). Biodegradation of Malachite Green Dye by Novel Isolated Bacillus Species AAV from Garden Soil, 88–95. https://doi.org/10.69626/csa.2024.0088

Muteeb, G., Alshoaibi, A., & Ansari, K. (2025). Experimental optimization and machine learning modeling for sustainable Congo red dye removal from wastewater using activated goat bone biochar. *Journal of Science: Advanced Materials and Devices*, *10*(3), 100947. https://doi.org/https://doi.org/10.1016/j.jsamd.2025.100947

Muteeb, G., Ansari, K., Eyvaz, M., Farhan, M., Aatif, M., Agrawal, D., … Dehghani, M.H. (2025). Removal of methylene blue (MB) dye from water and wastewater using acid-activated chicken bone in a batch adsorption process. *Scientific Reports*, *15*(1), 23098. https://doi.org/10.1038/s41598-025-08341-3

Pasipanodya, D., Seedat, N., Patel, B., & Roopchund, R. (2024). Production of hydrochar from the hydrothermal carbonisation of food waste feedstock for use as an adsorbent in removal of heavy metals from water. *Biomass Conversion and Biorefinery*. https://doi.org/10.1007/s13399-024-06097-w

Razia, S., Basavaraju, H.C., Taqui, S.N., Deepakumari, H.N., Mir, R.A., Syed, A.A., … Islam, S. (2025). Utilizing Industrial Fennel Seed Waste and Brilliant Green from Nutraceuticals for a Sustainable Wastewater Dye Adsorption System. *Rocznik Ochrona Środowiska*, 27.

Shukla, A.K., Alam, J., Mallik, S., Ruokolainen, J., Kesari, K.K., & Alhoshan, M. (2024). Optimization and prediction of dye adsorption utilising cross-linked chitosan-activated charcoal: response surface methodology and machine learning. *Journal of Molecular Liquids*, *411*, 125745.

Singh, R., Gaur, A., Soni, P., Jain, R., Pant, G., Kumar, D., … Ansari, K. (2025). A review of biofuels and bioenergy production as a sustainable alternative: opportunities, challenges and future perspectives. *Journal of Environmental Health Science and Engineering*, *23*(2), 23. https://doi.org/10.1007/s40201-025-00946-0

Waghmare, C., Ghodmare, S., Ansari, K., Alfaisal, F.M., Alam, S., Khan, M.A., & Ezaier, Y. (2024). Adsorption of methylene blue dye onto phosphoric acid-treated pomegranate peel adsorbent: Kinetic and thermodynamic studies. *Desalination and Water Treatment*, *318*, 100406. https://doi.org/https://doi.org/10.1016/j.dwt.2024.100406

Waghmare, C., Ghodmare, S., Ansari, K., Dehghani, M.H., Amir Khan, M., Hasan, M.A., … Zahmatkesh, S. (2023). Experimental investigation of H_3PO_4 activated papaya peels for methylene blue dye removal from aqueous solution: Evaluation on optimization, kinetics, isotherm, thermodynamics, and reusability studies. *Journal of Environmental Management*, *345*, 118815. https://doi.org/10.1016/j.jenvman.2023.118815